Chapter 2
Scientific Background

A colloidal system consists of two separate phases: a dispersed phase (or internal phase) and a continuous phase (or dispersion medium). The dispersed phase and the continuous medium can be in gas, liquid, and solid states. The dispersed-phase has a diameter of between approximately 1 and 1000 nm. Homogeneous mixtures with a dispersed phase in this size range may be called colloidal aerosols, colloidal emulsions, colloidal foams, colloidal suspensions, or hydrosols depending on varying combinations of dispersed phase and continuous phase.

A distinguishing feature of colloidal systems is that the contact area between dispersed phase and the dispersing medium is large. As a result, surface forces strongly influence dispersion behavior. By tailoring interactions between dispersed-phase, one can design colloids needed for specific applications. The stability, rheology, and other desired properties of colloids are controlled internally by the surface charge of the dispersed-phase and externally by the properties of the dispersing medium, such as temperature, pH, and ionic strength.

2.1 Surface Forces

The forces of charged colloids interacting through a liquid medium can be described by Derjaguin-Landau-Verwey-Overbeek (DLVO) theory [1, 2]. It combines the effects of the van der Waals attraction and the electrostatic repulsion due to the so-called double layer of counterions. Because of the markedly different distance dependency of the van der Waals and electrostatic interactions, the total force can show several minima and maxima with varying interparticle distance. Additional forces, such as structural force (solvation force) and hydrophobic force commonly occur in aqueous solutions. Considering the present experimental systems, the involved forces will be described: van der Waal force, electrostatic force, structural force and hydrophobic force.

Y. Zeng, *Colloidal Dispersions Under Slit-Pore Confinement*, Springer Theses,
DOI: 10.1007/978-3-642-34991-1_2, © Springer-Verlag Berlin Heidelberg 2012

2.1.1 Van der Waals Force

Van der Waals forces are a family of short-range forces, including the dipole–dipole force, dipole-induced dipole force, and dispersion forces. The expression of the van der Waals interaction between particles can follow the method by Hamaker [3], in which the net interaction energy is the integration of all pair contributions between two bodies. Thus the non-retarded van der Waals interaction energy of two spheres of radius R_1 and R_2 can be obtained as

$$V_{vdW}(D) = -\frac{A_H}{6}\left[\frac{2R_1R_2}{D^2+2(R_1+R_2)D} + \frac{2R_1R_2}{D^2+2(R_1+R_2)D+4R_1R_2} + \ln\left(\frac{D^2+2R_1D+2R_2D}{D^2+2(R_1+R_2)D+4R_1R_2}\right)\right] \tag{2.1}$$

where A_H is the Hamaker constant, R_1 and R_2 are the radius of particle 1 and 2, respectively, and D is the surface-to-surface distance, that is, $D = r - (R_1 + R_2)$ (r being the particle center-to-center distance).

The corresponding simplified expression of the van der Waals interaction energy of a particle approaching a surface is

$$V_{vdW}(D) = -\frac{A_H R_{norm}}{6D} \tag{2.2}$$

where R_{norm} is the normalized radius, which depends on the geometry used. In the case of sphere/flat geometry: $R_{norm} = R_{sphere}$, sphere/sphere geometry: $R_{norm} = R_1R_2/(R_1 + R_2)$. The van der Waals force can be obtained by differentiating the energy with respect to distance

$$F_{vdW} = -\frac{dV_{vdW}}{dD} = \frac{A_H R_{norm}}{6D^2} \tag{2.3}$$

The van der Waals force is always attractive between identical surfaces of the same materials, and can be repulsive between surfaces of dissimilar materials. Hamaker's method and the associated Hamaker constant A_H assumes that the interaction is pairwise additive and ignores the influence of an intervening medium between the two particles of interaction.

$$A_H = \pi^2 \times C \times \rho_1 \times \rho_2 \tag{2.4}$$

where ρ_1 and ρ_2 are the number of atoms per unit volume in two interacting bodies and C is the coefficient in the particle-particle pair interaction. The more advanced Lifshitz theory [4] has a same expression of the van der Waals energy but with consideration of the dielectric properties of the intervening medium, thus the Hamaker constant has a different value.

2.1.2 Electrostatic Force

The electrostatic force originates from the fact that most surfaces in contact with any liquid of high dielectric constant acquire a surface charge. The surface can either be charged by ionization of surface groups (e.g. silanol groups for glass or silica surfaces) or by adsorption of charged ions from the surrounding solution. This results in the development of a surface potential which attracts counterions from the surrounding solution and repels co-ions. In equilibrium, the surface charge is electrically neutralized by oppositely charged counterions in solution within some distance from the surface. The region near the surface of enhanced counterion concentration is called the electrical double layer (EDL) [1]. The EDL can be approximately sub-divided into two regions. Ions in the region closest to the charged wall surface are strongly bound to the surface. This immobile layer is called the Stern or Helmholtz layer. The region adjacent to the Stern layer is called the diffuse layer and contains loosely associated ions that are comparatively mobile. The whole electrical double layer, due to the distribution of the counterion concentration, results in the electrostatic screening of the surface charge.

The decay length of the diffuse electric double layer is known as the Debye screening length [5], κ^{-1}, which is purely a property of the electrolyte solution. The Debye length falls with increasing ionic strength of the solution. In totally pure water at pH 7, κ^{-1} is 960 nm, and in 1 mM NaCl solution κ^{-1} is 9.6 nm. The value κ is given by the relation

$$\kappa = \sqrt{\sum_i \rho_{\infty i} e_0^2 z_i^2 / \epsilon \epsilon_0 k_B T} \tag{2.5}$$

where $\rho_{\infty i}$ is the number density of ion i in the bulk solution, z_i is the valency of the ion i, e_0 is the elementary charge, ϵ_0 and ϵ are the permittivity of the vacuum and the solvent dielectric constant, respectively, and k_B is Boltzmann's constant.

The Debye length determines the range of the electrostatic double-layer interaction between two charged surfaces. The repulsive interaction between two equally charged surfaces is an entropic (osmotic) force. Actually, the electrostatic contribution to the net force is attractive. What maintains the diffuse double layer is the repulsive osmotic pressure between the counterions which forces them away from the surfaces and from each other so as to increase their configurational entropy. When bringing two equally charged surfaces together, one is therefore forcing the counterions back onto the surfaces against their osmotic repulsion, but favored by the electrostatic interaction. The former dominates and the net force is repulsive. Commonly speaking, when two charge surfaces approach each other, the electric double layers overlap and results in the so-called electric or electrostatic double layer repulsion force, even though the repulsion really arises from entropic confinement of the double layer ions.

The electrostatic interaction can be obtained by solving the Poisson-Boltzmann equation [6] for the potential distribution or counterion distribution in the liquid,

subject to suitable boundary conditions [5, 7]. These conditions are usually either constant surface potential if the concentration of counterions is constant as D is decreased (e.g. metal sols in a solution) or constant surface charge if the total number of counterions in liquid does not change (e.g. clay minerals). Using weak overlap approximation at constant potential [5], the free energy per unit area of interaction between two spheres is

$$W_{EL} = (64k_BT\rho_\infty\gamma_1\gamma_2/\kappa)e^{-\kappa D} \tag{2.6}$$

where γ is the reduced surface potential $\gamma = \tanh\left(\frac{ze\psi_0}{4k_BT}\right)$, ψ_0 is the potential on the surface.

Using Derjaguin approximation $F = 2\pi R_{norm} W$ [8], the expression of electrostatic force F between two spheres becomes

$$F_{EL} = (128\pi k_BT\rho_\infty R_{norm}\gamma_1\gamma_2/\kappa)e^{-\kappa D} \tag{2.7}$$

In the simplest case, $F_{EL} = (64\pi k_BT\rho_\infty R\gamma^2/\kappa)e^{-\kappa D}$ for two identically charged particles of radius R. This approximation is appropriate for surface potential between 30 and 100 mV. At low surface potentials, below 30 mV, the electrostatic force can be simplified with linear Poisson-Boltzmann approximation,

$$F_{EL} \approx 2\pi R\epsilon\epsilon_0\psi_0^2\kappa e^{-\kappa D} = 2\pi R q_f^2 e^{-\kappa D}/\kappa\epsilon\epsilon_0 \tag{2.8}$$

where the surface potential ψ_0 and surface charge density q_f are related by $q_f = \kappa\epsilon\epsilon_0\psi_0$. For more general case, the surface charge density is calculated by using the Grahame equation [5]

$$q_f = \sqrt{8\epsilon_0\epsilon k_BT I_{tot} N_A}\sinh\left(\frac{e_0\psi_0}{2k_BT}\right) \tag{2.9}$$

where I_{tot} is the bulk total ionic strength, $I_{tot} = \frac{1}{2N_A}\sum_{i=1}^{n}\rho_{\infty i}z_i^2$.

It should be noted that the above equations are accurate for surface separation beyond one Debye length. At small separation one has to use numerical solutions of the Poisson-Boltzmann equation to obtain the exact interaction potential, for which there are no simple and accurate expressions. The charge regulation due to the counterion binding needs to be taken into account, therefore the strength of the double layer interaction is always less than that obtained at constant surface charge condition and higher than that at constant surface potential.

Combining the van der Waals force and the electrostatic double layer force, the DLVO force between two particles or two surfaces in a liquid can be expressed as:

$$F(D) = F_{vdW}(D) + F_{EL}(D) \tag{2.10}$$

In contrast to the double layer force, the van der Waals force is mostly insensitive to electrolyte strength and pH. Additionally, the van der Waals force is greater than the double layer force at small separation since it is a power law interaction, whereas the double layer force remains finite or increases much more slowly within the same separation range. The interplay between these two forces has many important consequences, thus understanding the individual forces and their contributions is a good way to control the stability of the colloidal suspensions.

2.1.3 Depletion Force

The depletion force exists in the systems containing particles with different length scales or particles and non-adsorbing polymer coils or micelles. In this dissertation, the depletion force arises between a micrometer-sized silica particle and a flat silica plate immersed in a dispersion of silica nanoparticles or surfactant micelles. The nanoparticles/micelles can be called depletion agents. Depletion agents are excluded from a shell of thickness of their radius around the larger silica particle (or silica plate), called the depletion zone. When two larger particles or surfaces are brought together and the distance h between two larger particle surfaces is less than diameter of depletion agents, $h < 2R$, their depletion zones will overlap and the depletion agents are expelled from the gap between the larger particles. The absence of depletion agents in the gap leads to a density gradient and an osmotic pressure causing the attractive depletion force between the larger particle surfaces. The range of the attraction is directly related to the radius of depletion agent, whereas the strength is proportional to the concentration of the depletion agent. Asakura and Oosawa [9, 10] first calculated the force per unit area between two parallel plates as being equal to the osmotic pressure of the surrounding depletion agent with simplest hard sphere approach:

$$\frac{F_{dep}}{A} = -\rho k_B T \Theta(2R - h), \quad h < 2R \tag{2.11}$$

where Θ is the Heaviside function. The depletion force depends on the particle number density ρ and absolute temperature T of the surrounding depletion agent. And $\frac{F_{dep}}{A} = 0$, for $h \geq 2R$ (Fig. 2.1).

A detailed insight into depletion forces is important for studying the stability and phase behavior of colloidal suspensions and for the understanding of properties of polymer-colloid mixtures and other self-assembling phenomena in liquid dispersions.

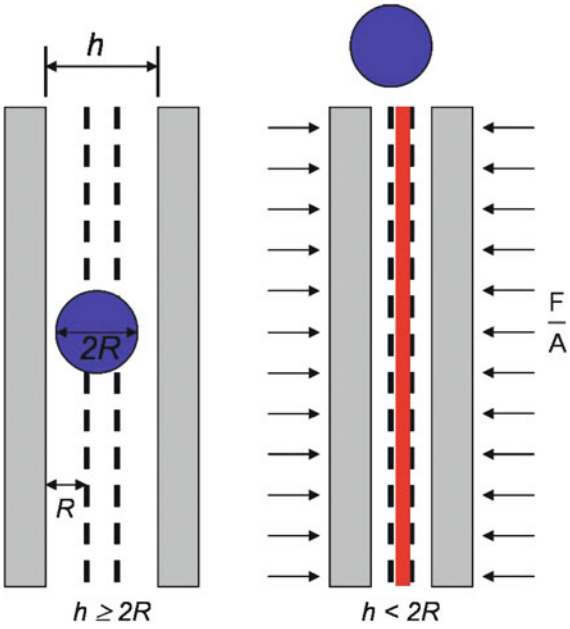

Fig. 2.1 When the distance between two surfaces is larger than the diameter of the depletion agents, $h \geq 2R$, the depletion agents can move into the gap and there is no depletion force acting on them. When the distance is small enough, $h < 2R$, the depletion agents are expelled from the gap and the net force acting on surfaces is equal to the pressure of the surrounding depletion agents

2.1.4 Structural force

Besides the depletion force, there is another non-DLVO force, called structural force or oscillatory force. It arises when the macroscopic surfaces are immersed in a relatively large concentration of the small colloidal particles. The structural force was first found by Israelachvili in the system of confined water molecules. The structural force is a generic feature also for colloidal particles, liquid crystals, and polyelectrolytes. These complex fluids can be considered as depletion agents for larger particles (surfaces). At large separation, the density of depletion agents in any highly restricted space is the same as that in bulk.

The density profile of depletion agents normal to a solid surface oscillates around the bulk density with a periodicity close to the distance of the depletion agent, and this oscillation extends several effective diameters of the depletion agent into the liquid. Within this range, the depletion agents are induced to order into quasi-discrete layers. When a neighboring surface approaches, the density distributions normal to both surfaces overlap and the depletion agents are squeezed out of the restricted space layer by layer so as to be accommodated between two surfaces. The variation of overlapping density profile with separation leads to an oscillating osmotic pressure.

The osmotic pressure as a function of separation is

$$P(h) = k_B T[\rho_s(h) - \rho_s(\infty)] \tag{2.12}$$

where $\rho_s(h)$ is the density of depletion agent at two surfaces separated by a distance of h and $\rho_s(\infty)$ is the corresponding density at isolated surface. Thus an osmotic pressure arises once there is a change in the depletion agent's density at the surfaces as the surfaces approach each other. $\rho_s(h)$ is higher than $\rho_s(\infty)$ only when surface separations are multiples of the distance of the depletion agents and lower when at intermediate separations. At large separations, $\rho_s(h)$ approaches the value of $\rho_s(\infty)$, the osmotic pressure is zero.

As the last layer of depletion agent is squeezed out, $\rho_s(h \to 0) \to 0$, the osmotic pressure approaches a finite value given by

$$P(h \to 0) = -k_B T \rho_s(\infty) \tag{2.13}$$

which means the force at contact is negative. Equation 2.13 has the same form as the depletion force. Therefore, the depletion force is considered as a special case of the oscillatory force in the limit of very small separations.

The attractive surface-liquid interaction and geometric constraining both have influence on the variation of the layering of depletion agents with separation, the latter being essential because layering is still observed even in the absence of the attractive surface-liquid interaction.

For simple spherical depletion agents between two smooth surfaces the structural force is usually a decaying oscillatory function of distance (Fig. 2.2). For depletion agents with asymmetric shapes, the resulting structural force may also have a monotonically repulsive or attractive component. Structural forces depend not only on the properties of the depletion agent but also on the chemical and physical properties of the confining surfaces, such as the hydrophobicity, the morphology and the deformability of the surfaces.

In general, the oscillatory structural force consists of a harmonic oscillation coupled with an exponential decay function, thus it can be written as

$$\frac{F_{osc}(h)}{R} = A \exp\left(-\frac{h}{\xi_f}\right) \cos\left(2\pi \frac{h}{\lambda_f} + \theta_f\right) + \text{offset} \tag{2.14}$$

where R is the radius of the colloidal probe, and h is the separation between two confining surfaces. The three important parameters characterizing the oscillations are the amplitude A, the wavelength λ_f, and the decay length ξ_f. The amplitude describes the interaction strength of the particles, wavelength indicates the interparticle distance of the layered structuring, and decay length tells the degree of the ordering. This function is similar as the bulk pair correlation function which is valid at large interaction distance. Strictly speaking, this equation should apply at relatively large separation because the additional contribution of nonstructural forces exists at small distance.

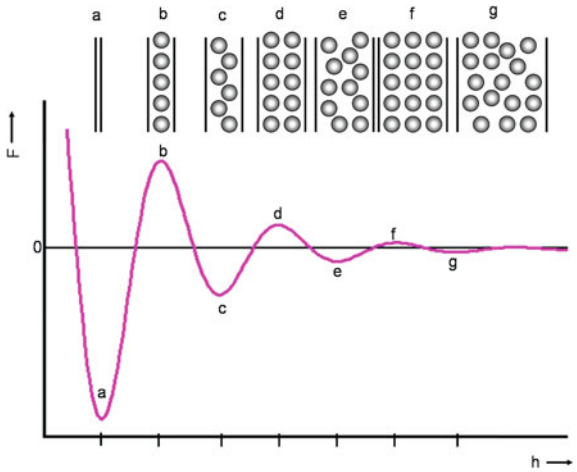

Fig. 2.2 Schematic illustration of the layering of spherical particles during the approach of two smooth surfaces and the corresponding measurable structural force. The density profile of particles changes with separation of two surfaces, resulting in different structuring of particles. At certain separation, particles are squeezed out of the gap to release the high inner pressure/force. The distance between two adjacent layers of particles relates to the inter-particle distance (illustration adopted from Israelachvili's book [5])

2.1.5 Hydrophobic Force

When using a hydrophobic surface, for example, replacing the solid substrate with a gas bubble or an other surface composed of hydrocarbons, the hydrophobic force plays a role in the system. The hydrophobic force describes the apparent repulsion between water and hydrophobic substances. Comparing to bond with hydrophilic molecules which have polar or ionic groups and hydrogen-bonding sites, water molecules have much less affinity to bond with the hydrophobic surface. The orientation of water molecules in contact with hydrophobic molecule is entropically unfavorable, therefore two hydrophobic molecules tend to come together and expel the water molecules into the bulk. This simple attractive force between hydrophobic molecules is favored because of the reduced total free energy of the system. Similarly, when water molecules are confined between hydrophobic surfaces, a net attractive force arises between the confining surfaces to expel the water molecules, which increases the translational and rotational entropy of water molecules and decreases the total free energy. Therefore, the attractive force, or hydrophobic force between hydrophobic surfaces is considered to be the consequence of water molecules migrating from a restricted space to the bulk water where there are unrestricted hydrogen-bonding opportunities and a lower free energy.

The attractive hydrophobic force is a long range force and much stronger than the van der Waals force [11–14]. It has a significant influence on the stability of colloids. Thus the force is needed to be taken into account when the system involves hydrophobic surfaces.

2.2 Theoretical Modelings

The developed theories are based on modeling by means of the integral equations of statistical mechanics [15], numerical simulations [16–18], and density-functional modeling [19–21]. As a rule, these approaches are related to complicated theoretical expressions or numerical procedures. The studies have shown that theoretical tools can describe oscillatory forces in a variety of model systems, such as hard spheres [16, 21, 22], polar fluids [23], liquid crystals [24], polyelectrolytes [25], and colloidal particles [17, 20]. In the case of nonionic micelles that can be modeled as hard spheres, Trokhymchuk et al. [22] proposed a quantitative analytical expression for the oscillatory force, which has been tested against both Monte-Carlo simulation data [22, 26] and data for stratifying free foam films [27].

2.2.1 Charged Particles

Based on Derjaguin-Landau-Verwey-Overbeck (DLVO) theory, a suspension of charged nanoparticles is modeled on an effective level which only includes the negatively charged silica nanoparticles explicitly [28–31]. Here, the electrostatic part of the DLVO potential is used [1]

$$u(r) = \tilde{Z}^2 e_0^2 \frac{\exp(-\kappa r)}{4\pi\epsilon_0\epsilon r} \tag{2.15}$$

where $Z = 4\pi(\sigma/2)^2 q_f$ is the total charge of a particle with diameter σ and surface charge density, q_f, which calculated from the Grahame Equation 2.9 with assuming the measured zeta potential ζ close to ψ_0.

In addition, $\tilde{Z}$ is the effective valency which is given by

$$\tilde{Z} = Z \exp(\kappa\sigma/2)/(1 + \kappa\sigma/2) \tag{2.16}$$

κ is the inverse Debye screening length, defined in Eq. 2.5 and can be also written as

$$\kappa = \sqrt{\frac{1}{\epsilon_0\epsilon k_B T}\left(\rho_c(z_c e_0)^2 + \sum_{k=1}^{K}\rho_k(z_k e_0)^2\right)} \tag{2.17}$$

where T is the temperature (set to 300 K), and ρ_c and z_c are the number density and valency of the counterions, respectively. The remaining sum refers to the additional salt ions. Assuming univalent counterions $|z_c| = 1$, the condition of charge neutrality between counterions and charged particles requires $\rho_c = |Z|\rho$. Equation 2.17 can then be rewritten as

$$\kappa = \sqrt{\frac{e_0^2}{\epsilon_0 \epsilon k_B T}(Z\rho + 2I_{salt}N_A)} \tag{2.18}$$

where $I_{salt} = \frac{1}{2N_A}\sum_{k=1}^{K}\rho_k(z_k)^2$ is the ionic strength of the additional salt, and N_A is Avogadro's constant.

For numerical reasons the soft sphere interaction $u_{SS}(r) = 4\epsilon_{SS}(\sigma/r)^{12}$ is added to the nanoparticles interaction which is, however, essentially negligible compared to the DLVO interaction energies at typical mean particle distances in this study.

Characteristic lengths as wavelength and decay length of bulk systems are extracted from bulk pair correlation functions $g_b(r)$. Within Monte Carlo (MC) simulations, $g_b(r)$ is determined using between 500 and 2000 particles depending on the volume fraction $\phi = (\pi/6)\rho\sigma^3$. Additionally, the integral equation for $g_b(r) \equiv h_b(r) + 1$ (with $h_b(r)$ being the total correlation function) consisting of the exact Ornstein-Zernike equation, $h(r_{12}) = c(r_{12}) + \rho\int dr^3 h(r_{13})c(r_{32})$ [32], combined with the approximate hypernetted chain (HNC) closure, $g(r) = \exp[-\beta u(r) + h(r) - c(r)]$ [33], is solved.

A convenient feature of using integral equations is that the asymptotic structure, that is, the dominant wavelength and correlation length of the function $h_b(r) = g_b(r) - 1$ in the limit $r \to \infty$ can be determined directly. This is done by analyzing the complex poles $q = \pm q_1 + iq_0$ of the structure factor $S_b(q) = 1 + \rho\tilde{h_b}(q)$ [19]. The pole with the smallest imaginary part determines the slowest exponential decay and thus yields an analytical description of the asymptotic behavior of $h_b(r)$ which reads

$$rh_b(r) = A_b exp(-q_0 r)cos(q_1 r - \theta_b), \quad r \to \infty \tag{2.19}$$

with $q_0 = \xi_b^{-1}$ playing the role of an inverse decay length (correlation length) and $q_1 = 2\pi/\lambda_b$ determining the wavelength of the oscillation. q_0 and q_1 can be also determined from the MC data by plotting the function $\ln(r\,|h_b(r)|)$. Wavelength and correlation length then follow from the oscillations and the slope of the straight line connecting the maxima at large r.

The HNC and MC results for wavelength in bulk λ_b as a function of the particle volume fraction ϕ are given in the main part of Fig. 2.3, showing that the two approaches are in good agreement. This is consistent with the observations previously reported [34] and justifies the use of HNC in the bulk system.

DFT [19, 20] predicts that, for sufficiently large h allowing a bulk-like region in the middle of the pore, the microscopic density profile should decay as $\rho(z) - \rho_b \to A_\rho exp(-q_0 z)cos(q_1 z - \theta_\rho)$, where q_0 and q_1 are exactly the same as in the bulk system at equal chemical potential μ (with bulk particle number density ρ_b), whereas the amplitude A_ρ and θ_ρ depend on the nature of fluid-wall (particle-confining surface) interactions. The same asymptotic behavior is expected for the so-called normal solvation pressure, $f(h) = P_{zz}(h) - P_{bulk}$.

The confined system modeled first by two infinite plane parallel, smooth, uncharged surfaces separated by a distance h along the z-direction [28, 30], fluid-wall (particle-confining surface) interaction is chosen to be purely repulsive and read as

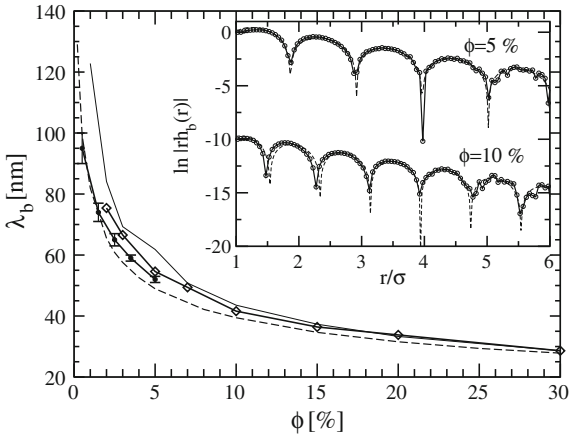

Fig. 2.3 Dominant wavelength λ_b characterizing $h_b(r) = g_b(r) - 1$ as a function of the volume fraction according to HNC (*solid line*) and MC (*diamonds*). Also shown are the HNC data for λ_s [28] (*dashed line*) and the corresponding SANS data for λ_s [30] (*filled circles*, with error bars). The inset shows two MC results for the function $\ln(r\,|h_b(r)|)$ (*circles*). The asymptotic fit functions are plotted as *dashed lines*

$$u_{\mathrm{FS}}^{\mathrm{SW}}(z) = \frac{4}{5}\pi\epsilon_{\mathrm{w}}\left(\frac{\sigma}{z}\right)^9 \tag{2.20}$$

The MC simulation in the grand canonical (GC) ensemble can be employed to investigate the confined systems, that is, at constant temperature, wall separation, box area parallel to the walls, and constant chemical potential μ [28, 35]. Furthermore, the inverse Debye length should be fixed at the value corresponding to the bulk volume fraction. The solvation pressure $f(h) = P_{zz}(h) - P_b$ with P_b being the bulk pressure and $P_{zz}(h)$ the normal component of the pressure tensor [35] exhibits oscillations with varying surface separation. This quantity is related to the oscillatory forces of the AFM experiment via Derjaguin's approximation [21]. The functions $f(h)$ are fitted according to the expression

$$\tilde{f}(h) = A_{\mathrm{f}} \exp\left(-\frac{h}{\xi_{\mathrm{f}}}\right) \cos\left(\frac{2\pi h}{\lambda_{\mathrm{f}}} - \theta_{\mathrm{f}}\right) \tag{2.21}$$

with λ_f and ξ_f being the wavelength and decay length, respectively.

In the whole particle concentration range considered, the oscillatory asymptotic decay of *f(h)* (determined by a wavelength λ_f) is indeed well described by the leading bulk wavelength (and correlation length), implying $\lambda_f = \lambda_b$. This is particularly well-demonstrated by the logarithmic representation in the inset of Fig. 2.4. Thus, the GCMC simulation results for the charged silica particles confirm the DFT predictions. As Eq. 2.19 derived from Ornstein-Zernike theory Eq. 2.21 is only valid for $h \to \infty$. However the asymptotic expression is found to provide a good approximation of

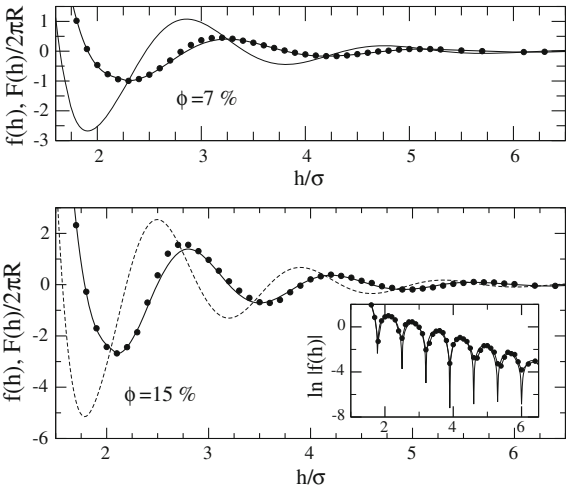

Fig. 2.4 Two examples of the solvation pressure *f(h)* as obtained by GCMC (*filled circles*) together with the asymptotic fits (*solid line*) obtained with the bulk values of $q_1 = 2\pi/\lambda_b$ and q_0. Included are the resulting structural forces $F(h)/2\pi R$ (*dashed line*). The inset shows a logarithmic plot of *f(h)*

the oscillations already at remarkably small wall separations. The full curve is well described by the asymptotic formula already after the first minimum at $h = h_{min}$. For smaller separations $h \leq h_{min}$, a cubic polynomial fit is used:

$$\tilde{f}(h) = a_0 + a_1 h + a_2 h^2 + a_3 h^3 \tag{2.22}$$

The coefficients are adjusted such that both the pressure and its derivative are continuous at h_{min}. Then, an accurate fit formula for *f(h)* can be found by immediately integrating *f(h)* [21] to obtain the solvation force $F(h)/2\pi R$, results for which are included in Fig. 2.4.

In order to obtain the impact of surface potential on the other quantities of the solvation forces, i.e. amplitude and phase shift, which is predicted by the DFT, the confined system is modeled by two infinite plane parallel, smooth, charged surfaces separated by a distance h along the z-direction [31]. Their surface potential mimics the experimental conditions. A simplest version of linearized Poisson-Boltzmann (PB) theory is first employed

$$u_1(z) = W_S \exp\left(-\kappa\left(\frac{h}{2} - z\right)\right) + W_S \exp\left(-\kappa\left(\frac{h}{2} + z\right)\right) \tag{2.23}$$

The decay of potential is determined by the bulk Debye screening length κ and the wall charge only come into play through a prefactor $W_S = 64\pi\epsilon_0\epsilon\gamma_f\gamma_s R\,(k_B T/e_0)^2$, where $\gamma_{F/S} = \tanh\left(e_0\psi_{F/S}/4k_B T\right)$, $\psi_{F/S}$ is the surface potential of the fluid particles *(F)* and the solid walls *(S)*, and R is the radius of the fluid particle, $R = \sigma/2$. This model has the consequence that the oscillations of the normal pressure become weakened with increasing $|\psi_S|$, which is in contradiction to the experiment.

Thus a modified fluid-wall potential is developed. It takes additional wall counterions into account which change the screening between charged walls and colloidal particles. The expression of a silica ion and one of the charged walls is read as

$$u_{\mathrm{FS}}^{\mathrm{LSA}}(z) = 64\pi\epsilon_0\epsilon\gamma_{\mathrm{F}}\gamma_{\mathrm{S}}R\left(\frac{k_BT}{e_0}\right)^2 \exp\left[-\kappa_{\mathrm{W}}(z-R)\right] \tag{2.24}$$

where the screening parameter depends on ψ_S and is space-dependent,

$$\kappa_{\mathrm{W}}(z) = \sqrt{\frac{e_0^2}{\epsilon_0\epsilon k_BT}\left(Z\rho + 2I_{salt}N_{\mathrm{A}} + \frac{|q_{\mathrm{S}}|}{e_0 z}\right)} \tag{2.25}$$

and the confining surface charge density q_{S} is related to the surface potential via the Grahame equation.

The total fluid-wall interaction is therefore given by

$$u_{\mathrm{FS}}(z) = u_{\mathrm{FS}}^{\mathrm{LSA}}(h/2-z) + u_{\mathrm{FS}}^{\mathrm{LSA}}(h/2+z) + u_{\mathrm{FS}}^{\mathrm{SW}}(h/2-z) + u_{\mathrm{FS}}^{\mathrm{SW}}(h/2+z) \tag{2.26}$$

where $u_{\mathrm{FS}}^{\mathrm{LSA}}$ and $u_{\mathrm{FS}}^{\mathrm{SW}}$ are given by Eqs. 2.24 and 2.20, respectively. This induces a non-monotonic behavior of the fluid-wall interaction potential as a function of the wall charge.

2.2.2 Nonionic Surfactant Micelles

Using the Derjaguin's approximation, one can express the surface force, F, between a spherical particle and a planar plate in the form:

$$F(h) = 2\pi\ RW(h) \tag{2.27}$$

where R is the particle radius; h is the surface-to-surface distance between the particle and the plate; $W(h)$ is the interaction energy per unit area of a plane-parallel liquid film of thickness h. In the considered case of nonionic surfactant micelles, W can be expressed as a sum of contributions from the van der Waals forces, W_{vdW}, and oscillatory structural forces due to the surfactant micelles, W_{osc} [5, 27]

$$W(h) = W_{osc} + W_{vdW} = W_{osc} - \frac{A_H}{12\pi h^2} \tag{2.28}$$

The surface charge of the confining surfaces can be neglected, since confining surface charge would not change the oscillation wavelength and decay length, but increase the amplitude w_0 [20].

The combination of Eqs. 2.27 and 2.28 yields

$$F = 2\rho R \frac{k_B T}{d^2} \left(\frac{W_{osc} d^2}{k_B T} - \frac{A_H}{12\pi (h/d)^2 k_B T} \right) \tag{2.29}$$

where d is the micelle diameter; h/d is the dimensionless surface-to-surface distance. Furthermore, the expression for W_{osc} due to Trokhymchuk et al. [22] is used:

$$\frac{W_{osc} d^2}{k_B T} = -\frac{p_{hs} d^3}{k_B T}(1 - h/d) - \frac{2\sigma_{hs} d^2}{k_B T}, \quad 0 \leq h/d < 1 \tag{2.30}$$

$$\frac{W_{osc} d^2}{k_B T} = w_0 \cos(\omega h/d + \varphi_1) \exp^{-qh/d} + w_1 \exp^{\delta(1-h/d)}, \quad h/d \geq 1 \tag{2.31}$$

where p_{hs} is the pressure of a hard-sphere fluid expressed through the Carnahan-Starling formula [36], and σ_{hs} is the scaled-particle-theory [37] expression for the excess surface free energy of a hard-sphere fluid:

$$\frac{p_{hs} d^3}{k_B T} = \frac{6}{\pi} \phi \frac{1 + \phi + \phi^2 - \phi^3}{(1 - \phi)^3} \tag{2.32}$$

$$\frac{\sigma_{hs} d^2}{k_B T} = -\frac{9}{2\pi} \phi^2 \frac{1 + \phi}{(1 - \phi)^3} \tag{2.33}$$

The parameters w_0, ω, φ_1, q, w_1 and δ in Eq. 2.31 depend on the hard-sphere (micelle) volume fraction, ϕ, as follows [22]

$$w_0 = 0.57909 + 0.83439\phi + 8.65315\phi^2 \tag{2.34}$$

$$\omega = 4.45160 + 7.10586\phi - 8.30671\phi^2 + 8.29751\phi^3 \tag{2.35}$$

$$q = 4.78366 - 19.64378\phi + 37.37944\phi^2 - 30.59647\phi^3 \tag{2.36}$$

$$w_1 = \frac{2\sigma_{hs} d^2}{k_B T} - w_0 \cos(\omega + \varphi_1) \exp(-q) \tag{2.37}$$

$$\varphi_1 = 0.40095 + 2.10336\phi, \delta = \frac{\pi_1}{w_1} \tag{2.38}$$

where

$$\pi_1 = \frac{6}{\pi}\phi \exp\left(\frac{\Delta\mu_{hs}}{k_B T}\right) - \frac{p_{hs} d^3}{k_B T} - \pi_0 \cos(\omega + \varphi_2)\exp(-q) \tag{2.39}$$

$$\frac{\mu_{hs}}{k_B T} = \phi \frac{8 - 9\phi + 3\phi^2}{(1-\phi)^3} \tag{2.40}$$

$$\pi_0 = 4.06281 - 3.10572\phi + 76.67381\phi^2 \tag{2.41}$$

$$\varphi_2 = -0.39687 - 0.3948\phi + 2.3027\phi^2 \tag{2.42}$$

The parameters w_0, ω, and q defined by Eqs. 2.34–2.36 characterize, respectively, the amplitude, wavelength and decay length of the oscillations (see Eq. 2.31). The last term in Eq. 2.31 ensures the correct height of the first (the highest) maximum [22]. Note that for a hard sphere fluid, the amplitude, wavelength and decay length of the oscillations depend on the particle volume fraction, ϕ, in accordance with Eqs. 2.34–2.36.

Equation 2.29, along with Eqs. 2.30–2.42, determines the theoretical dependence $F(h, \phi)$ at given colloidal probe radius, R, and micelle diameter, d. In particular, for a given micelle volume fraction, ϕ, p_{hs}, σ_{hs}, w_0, ω, q, μ_{hs}, π_0 can be first calculated, and φ_2 from Eqs. 2.32–2.36 and Eqs. 2.40–2.42; after that, w_1, φ_1, π_1 and δ can be calculated from Eqs. 2.37–2.39; next W_{osc} is computed from Eqs. 2.30–2.31, and finally F, from Eq. 2.29.

The fitting procedure is as follows. The experimental force, F_{exp} is given as a function of the experimental distance, $h_{exp} = h + \Delta h$, where h is the theoretical distance and Δh is the difference between the positions of the experimental and theoretical coordinate origins on the h-axis. The fitting by means of the least-squares method consists of numerical minimization of the following merit function:

$$\Phi(\Delta h, \phi) = \sum_{\mathrm{i}} \left[F\left(h^i_{\mathrm{exp}} - \Delta h, \phi\right) - F^i_{\mathrm{exp}}\left(h^i_{\mathrm{exp}}\right)\right]^2 \tag{2.43}$$

where $F^i_{\mathrm{exp}}\left(h^i_{\mathrm{exp}}\right)$ is the set of experimental data numbered by the index i, and the summation is carried out over all experimental points. It is important to note that in the fitting procedure, the points from the non-equilibrium portions of the experimental curves have to be excluded, because the theoretical curve gives the equilibrium force-versus-distance dependence.

When ϕ is known, the variation of Δh is equivalent to a simple horizontal translation of the experimental curve with respect to the theoretical one, the latter being uniquely determined. The minimization of Φ with respect to Δh corresponds to the best coincidence of the two curves. When ϕ is not known, both Δh and ϕ should be

varied to minimize numerically Φ in Eq. 2.43, and to find the best fit. When calculating the theoretical curves, in Eq. 2.29 the value $A_H = 7 \times 10^{-21}$ J of the Hamaker constant for silica/water/silica films is used [5]. The effect of van der Waals forces is essential only at the lowest investigated micellar concentrations, where the oscillatory amplitude w_0 is relatively small.

References

1. Verwey, E. J. W., & Overbeek, J. T. G. (1948). *Theory of stability of lyophobic colloids*. Amsterdam: ELSEVIER.
2. Derjaguin, B. V., & Landau, L. (1941). *Acta Physicochim URSS*, *14*, 633.
3. Hamaker, H. C. (1937). *Physica*, *4*, 1058–72.
4. Lifshitz, E. M. (1956). *Soviet Physics JETP USSR*, *2*, 73–83.
5. Israelachvili, J. N. (1992). *Intermolecular and surface forces*. London: Academic Press.
6. Russel, W., Saville, D., & Schowalter, W. (1989). *Colloidal dispersions*. Cambridge, UK: Cambridge University Press.
7. Hutter, R. J. (2002). *Foundations of colloid science*. Oxford: Oxford University Press.
8. Derjaguin, B. V. (1934). *Kolloid Z*, *69*, 155–64.
9. Asakura, S., & Oosawa, F. (1954). *Journal of Chemical Physics*, *22*, 1255–1256.
10. Asakura, S., & Oosawa, F. (1958). *Journal of Polymer Science*, *33*, 183–192.
11. Israelachvili, J., & Pashley, R. (1982). *Nature*, *300*, 341–342.
12. Israelachvili, J., & Pashley, R. (1984). *Journal of Colloid and Interface Science*, *98*, 500–514.
13. Rabinovich, Y., & Derjaguin, B. (1988). *Colloids and Surfaces*, *30*, 243–251.
14. Claesson, P., & Christenson, H. (1988). *Journal of Physics and Chemistry*, *92*, 1650–1655.
15. Attard, P., & Parker, J. (1992). *Journal of Physics and Chemistry*, *96*, 5086–5093.
16. Blawzdziewicz, J., & Wajnryb, E. (2005). *Europhysics Letters*, *71*, 269–275.
17. Trokhynichuk, A., Henderson, D., Nikolov, A., & Wasan, D. (2005). *Langmuir*, *21*, 10240–10250.
18. Schoen, M., & Klapp, S. H. L. (2007). *Nanoconfined fluids. Soft matter between two and three dimensions*. New York: Wiley.
19. Evans, R., Henderson, J., Hoyle, D., Parry, A., & Sabeur, Z. (1993). *Molecular Physics*, *80*, 755–775.
20. Grodon, C., Dijkstra, M., Evans, R., & Roth, R. (2005). *Molecular Physics*, *103*, 3009–3023.
21. Gotzelmann, B., Evans, R., & Dietrich, S. (1998). *Physical Review E*, *57*, 6785–6800.
22. Trokhymchuk, A., Henderson, D., Nikolov, A., & Wasan, D. (2001). *Langmuir*, *17*, 4940–4947.
23. Klapp, S., & Schoen, M. (2002). *Journal of Chemical Physics*, *117*, 8050–8062.
24. Schoen, M., Gruhn, T., & Diestler, D. (1998). *Journal of Chemical Physics*, *109*, 301–311.
25. Jonsson, B., Broukhno, A., Forsman, J., & Akesson, T. (2003). *Langmuir*, *19*, 9914–9922.
26. Kralchevsky, P., & Denkov, N. (1995). *Chemical Physics Letters*, *240*, 385–392.
27. Basheva, E. S., Kralchevsky, P. A., Danov, K. D., Ananthapadmanabhan, K. P., & Lips, A. (2007). *Physical Chemistry Chemical Physics*, *9*, 5183–5198.
28. Klapp, S. H. L., Qu, D., & von Klitzing, R. J. (2007). *Journal of Physical Chemistry B*, *111*, 1296–1303.
29. Klapp, S. H. L., Grandner, S., Zeng, Y., & von Klitzing, R. (2008). *Journal of Physics: Condensed Matter*, *20*, 494232.
30. Klapp, S. H. L., Zeng, Y., Qu, D., & von Klitzing, R. (2008). *Physical Review Letters*, *100*, 118303.
31. Grandner, S., Zeng, Y., von Klitzing, R., & Klapp, S. H. L. (2009). *Journal of Chemical Physics*, *131*, 154702.

32. Ornstein, L., & Zernike, F. (1914). *Proceedings of the Academy of Sciences Amsterdam*, *17*, 793.
33. Hansen, I. R., & McDonald, J. P. (2006). *Theory of simple liquids* (3rd ed.). Amsterdam: Academic Press.
34. Hopkins, P., Archer, A., & Evans, R. (2005). *Physical Review E*, *71*, 027401.
35. Schoen, M., Klapp, S. H. L (2007). *Reviews in computational chemsitry* (Vol. 24). New Jersey: WILEY-VCH.
36. Carnahan, N., & Starling, K. (1969). *Journal of Chemical Physics*, *51*, 635.
37. Reiss, H., Frisch, H., Helfand, E., & Lebowitz, J. (1960). *Journal of Chemical Physics*, *32*, 119–124.

http://www.springer.com/978-3-642-34991-1

Colloidal Dispersions Under Slit-Pore Confinement

Zeng, Y.

2012, XX, 124 p.,
ISBN: 978-3-642-34991-1